ECCOMAS Congress 2016
VII European Congress on Computational Methods in Applied Sciences and Engineering
M. Papadrakakis, V. Papadopoulos, G. Stefanou, V. Plevris (eds.)
Crete Island, Greece, 5–10 June 2016

NEAR-WALL BEHAVIOUR OF IMPLICIT LARGE EDDY SIMULATIONS

Ioannis W. Kokkinakis[1], **and Dimitris Drikakis**[1]

[1] University of Strathclyde
Glasgow, G1 1XQ, UK
e-mail: {ioannis.kokkinakis, dimitris.drikakis}@strath.ac.uk

Keywords: Implicit Large Eddy Simulation (ILES), turbulent boundary layers, compressible flows.

Abstract. *This paper investigates the accuracy of implicit large eddy simulations (ILES) in compressible turbulent boundary layers (TBL). ILES are conducted in conjunction with Monotonic Upstream-Centred Scheme for Conservation Laws (MUSCL) and Weighted Essentially Non-Oscillatory (WENO), ranging from 2^{nd} to 9^{th}-order. The excess artificial dissipation occurring at low Mach numbers is counter-balanced by using low Mach corrections. The study concludes that high-order ILES provide accurate predictions of TBL even on relatively coarse grids.*

1 INTRODUCTION

Design processes in engineering applications require satisfying various degrees of constraints in order to adhere to design quality standards. Through careful planning and availability of instrumentation/apparatus that conform to the necessary specifications, experimental results can indeed assist considerably during the design stage. However, most experiments are deemed cumbersome and require considerable time to plan, execute and later analyse. This is particularly true when a design cycle or optimization approach is required early on in the design phase. Furthermore, availability of diagnostic instrumentation limits the amount of useful information that can be extracted.

Computational methods offer the possibility of a high turnover of results and ample amounts of available data, allowing for a plethora of variations to the initial design of a product to be investigated. Though computational methods are increasingly becoming more popular and widely used, particularly in the early-on design phase of many engineering products, they are still treated with some caution and due care as the solutions provided can contain significant inaccuracies. These are caused mostly by the number of assumptions associated with turbulence modelling as well as the excessive numerical dissipation of schemes particularly when simulations are performed on coarse grids.

Though conducting ILES is deemed too computationally costly for use in most engineering design projects, it is only now, with the availability of evermore increasing computational power, that ILES is in its "infancy" in terms of use in wider industrial applications. Increasing the applicability of ILES requires increasing their accuracy in coarse grid simulations.

Therefore, in this paper, the accuracy of high-order, shock-capturing schemes along with any caveats, are investigated in conjunction with ILES to near-wall turbulent boundary layer (TBL) flows. The effects of numerical dissipation for schemes with accuracy ranging from 2^{nd} to 9^{th}-order are investigated both in subsonic and supersonic TBL. The results show that higher order ILES schemes are particularly well suited for simulating TBL and prove resilient to the excess artificial dissipation in low Mach flow regions.

2 METHODOLOGY

The in-house block-structured grid code CNS3D is used to solve the Navier-Stokes equations using a finite volume Godunov-type method for the convective terms. The inter-cell numerical fluxes of the convective terms are calculated by solving the Riemann problem using the reconstructed values of the conservative variables at the cell interfaces. The reconstruction stencil is a one-dimensional swept unidirectional stencil. The Riemann problem is solved using the so-called "Harten, Lax, van Leer, and (the missing) Contact" (HLLC) approximate Riemann solver [1]. Two different flux limiting approaches have been implemented in conjunction with the HLLC solver, namely the: (i) Monotone Upstream-centred Schemes for Conservation Laws (MUSCL) and (ii) Weighted-Essentially-Non-Oscillatory (WENO). In particular, the following schemes are examined:

- MUSCL piecewise linear 2^{nd} order Monotonized Central (MC) limiter [2];
- MUSCL 3^{rd} (M3) and 5^{th} (M5) order limiters [3];
- WENO 5^{th} (W5) and 9^{th} (W9) order schemes [4].

The accuracy of the above schemes, as well as of any other, can be further improved in the low subsonic region of transitional/turbulent boundary layers by implementing low-Mach corrections [5] (henceforth labelled LM). This essentially involves an additional numerical re-

construction step of the velocity vector via a progressive central differencing of the velocity components. LM corrections ensure a balanced distribution of dissipation of kinetic energy in the limit of zero Mach number, thus extending the validity of compressible flow codes to Mach numbers as low as 10^{-5}, and are particularly required for schemes providing accuracy less than 5^{th}-order [6]. The viscous terms are discretized by a second-order central scheme. The solution is advanced in time by using a five-stage (fourth-order accurate) optimal strong-stability-preserving Runge-Kutta method [7]. Further details of the numerical aspects of the code are given in [6] and [14] and references therein.

3 CHANNEL FLOW

The fully turbulent channel flow test-case has long been established as one of the major "canonical" flow problems used to perform detailed validation of numerical/computational methods. A detailed investigation of the accuracy of a number of popular numerical schemes, originally designed for shock-capturing, was carried out in [6] with respect to a weakly-compressible, turbulent channel flow. The specific objectives were: (i) to investigate the accuracy of the Monotone Upstream-centred Scheme for Conservation Laws (MUSCL) 2^{nd} to 5^{th}-order, and the Weighted Essentially Non-Oscillatory (WENO) 5^{th} to 9^{th}-order accurate flux limiter schemes against DNS data; (ii) to examine the effects of the low Mach correction on the accuracy of the MUSCL and WENO schemes; and (iii) to compare the numerical schemes with respect to their computational cost.

3.1 Case Parameters

The numerical assessment has been made using the incompressible DNS data of Moser et al. [8], corresponding to a friction Reynolds number of $Re_\tau = 395$ based on the friction velocity (u_τ) and channel half-height. Previous studies concerning compressible, turbulent channel flows have been conducted at Mach numbers of 0.4 (quasi-incompressible), however, to examine the effects of the numerical schemes with and without low Mach correction, we consider here a Mach number 0.2.

The size of the non-dimensional domain ($L_x \times L_y \times L_z$) is ($2\pi \times 2 \times \pi$) in the streamwise (x), wall normal (y) and spanwise (z) directions, respectively. In the streamwise and spanwise directions, periodic boundary conditions are employed, while in the wall normal direction an adiabatic no-slip wall condition is applied.

In Duan et al. [9], it was shown that many of the scaling relations used to express adiabatic compressible boundary-layer statistics in terms of incompressible boundary layers hold for non-adiabatic cases too. Wall cooling slightly enhances compressibility effects and increases the coherency of turbulent structures, however, its effects remain insignificant even for a supersonic turbulent channel flow. In the compressible DNS channel flow simulations of [10] and [11], it was shown that decreasing the wall temperature leads to higher skin friction. In the present study, the adiabatic wall condition was employed in order to examine the accuracy of the numerical methods unhindered by external heat transfer effects, thus obtaining a more meaningful comparison to the incompressible DNS. The streamwise velocity profile is given by a laminar (Poiseuille) parabolic profile with a white noise perturbation of 10% superimposed. Here we will summarize the key findings made using results only from the finest grid composed of 128^3 cells. A grid convergence study can be found in [6].

3.2 Results

The three-dimensional turbulent structures obtained from different simulations are shown by plotting the iso-surfaces of *Q*-criterion [12] in Figure 1 and Figure 2 for the schemes with-

out and with the LM correction, respectively. The *Q*-criterion is an indication of vorticity prevailing over strain and thus represents vortex cores.

The iso-surfaces reveal, in a qualitative manner, the ability of the different schemes to resolve turbulent structures. Note that for the calculation of *Q*-criterion, the velocity field is non-dimensionalized by the bulk velocity and the spatial dimensions by the channel half-height. It is clearly evident that as the order of accuracy of the reconstruction increases, more turbulent structures are resolved. For the same (5^{th}) order of accuracy, the W5 scheme resolves more turbulent structures than M5. MUSCL schemes are designed to satisfy positivity-preserving criterion in the framework of the total variation diminishing (TVD) condition, which inevitably leads to more dissipative schemes.

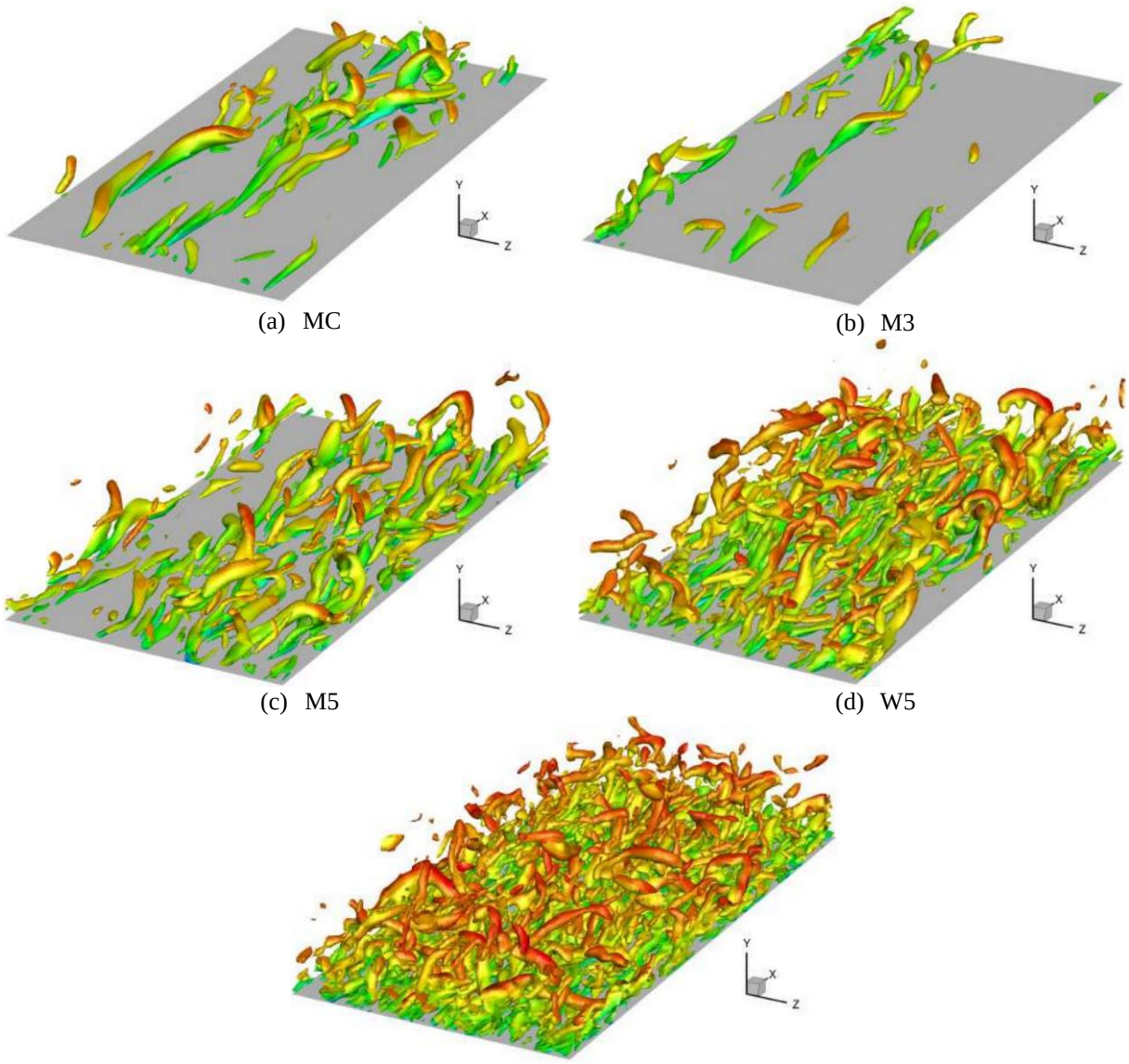

(a) MC (b) M3

(c) M5 (d) W5

(e) W9

Figure 1: *Q*-criterion iso-surfaces on 128^3 grid (iso-value=0.5 coloured by streamwise velocity).

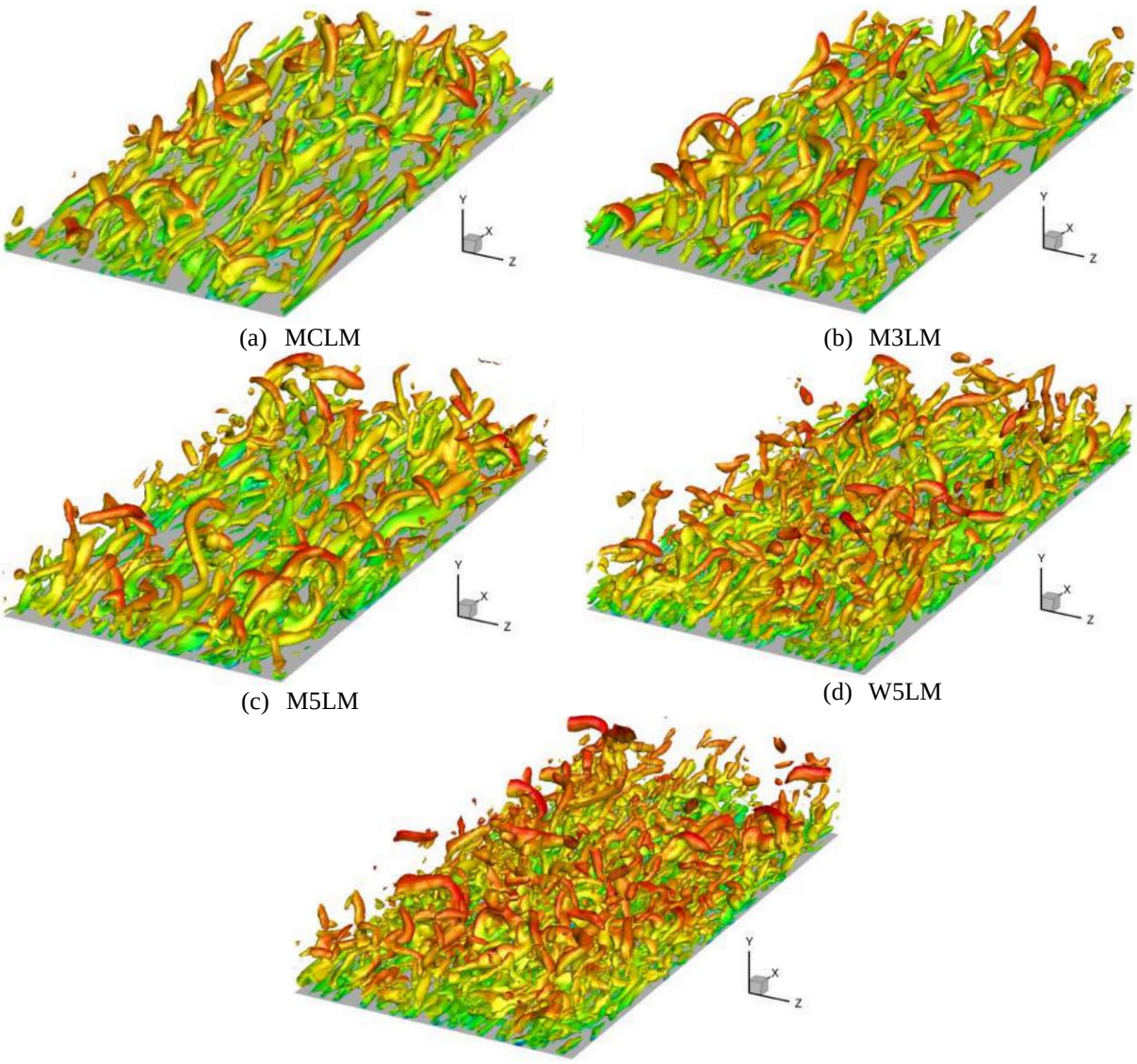

(a) MCLM (b) M3LM

(c) M5LM (d) W5LM

(e) W9LM

Figure 2: *Q*-criterion iso-surfaces on 128^3 grid (iso-value=0.5 coloured by streamwise velocity) using the low-Mach correction [5].

Application of the LM correction results in a remarkable improvement for the 2nd, 3rd and 5th-order schemes (Figure 2), enabling much finer turbulent scales to be resolved. As the order of the scheme decreases, hence the numerical dissipation increases, the greater the improvement the LM correction provides.

The W9 scheme is found to give the most turbulent-like solutions. As the W9 scheme is the least dissipative, the addition of the LM correction does not offer any significant improvement. In fact, it is shown later that it can actually result in less accurate solutions by amplifying the dispersive errors originating from the truncation error terms (odd order terms) of a dispersive dominant scheme.

The results also reveal the mechanism by which the generated vorticity produced in the viscous layer is subsequently "ejected" due to low speed streaks into the outer boundary layer, thus creating and sustaining turbulence. This mechanism is responsible for the production of hairpin vortices that get stretched by the ambient shear. These streamwise elongated vortices have also been reported by previous (incompressible) ILES studies [13].

Figure 3 shows the velocity profiles in wall units obtained by the different numerical schemes examined. The LM correction provides a significant improvement to the MC, M3 and M5 schemes and, to a lesser degree, the W5 scheme. In contrast, the LM correction slightly deteriorates the profile of the W9. The reason is that the W9 scheme is the least dissipative and most dispersive of the schemes examined. As a result, the LM correction triggers locally entropy-violating solutions which tend to reduce the numerical dissipation of a scheme. So, if the numerical dispersion of the scheme becomes significantly greater to the dissipation, it can actually have an adverse effect on the accuracy of the scheme.

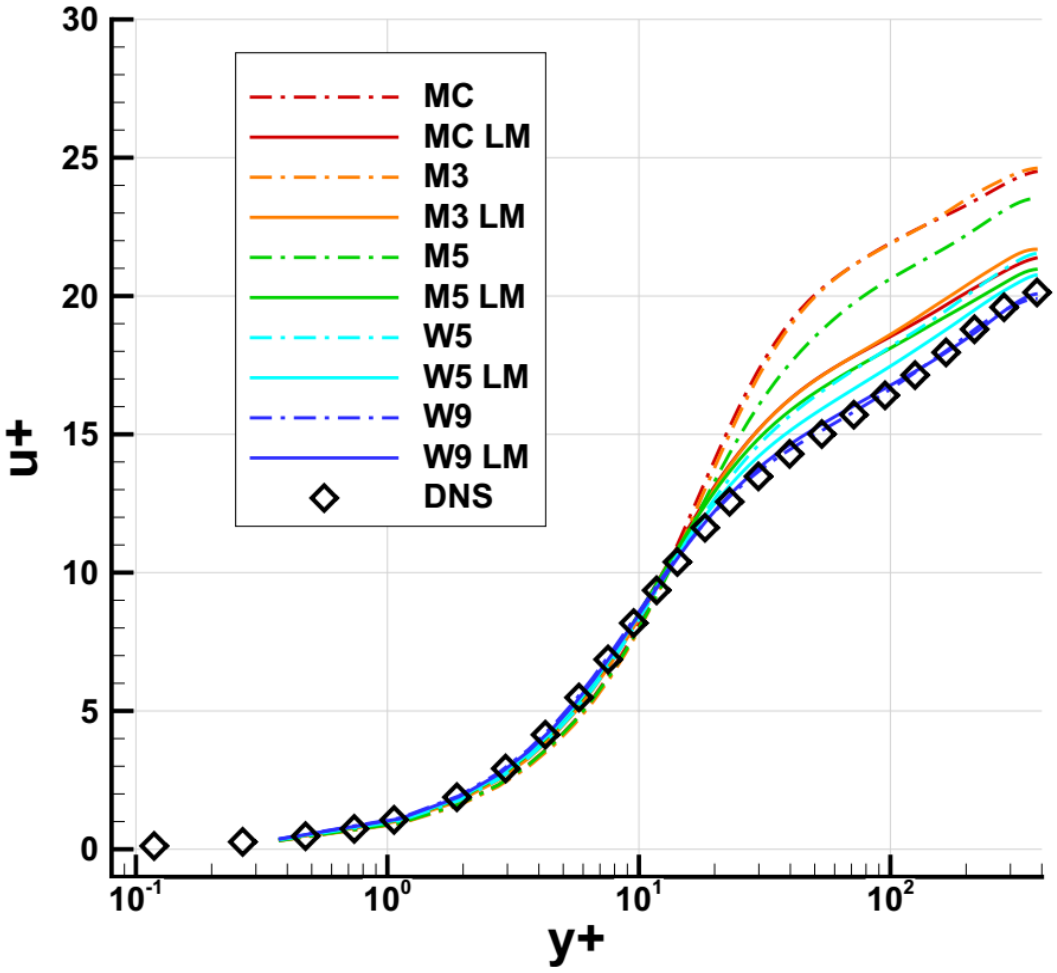

Figure 3: Velocity profiles in wall units for the different schemes.

The results obtained for the Reynolds stresses (RS) (Figure 4) reveal that the most accurate solution is obtained by the W9 scheme. The LM correction significantly improves the accuracy of all schemes apart from W9. The lower the order of accuracy of the scheme is, the greater the effect of the LM correction becomes. The W5 scheme gives better results than M5 for the $RS(u'u')$, $RS(v'v')$ and $RS(u'v')$, while similar results are obtained for $RS(v'v')$ and $RS(w'w')$ when M5 is used with LM corrections (M5LM). Overall, the W5 and W9 perform better than any of the MUSCL schemes and provide extremely accurate results.

The most noticeable result here is the significant over-prediction of the $RS(u'u')$ and under-prediction of $RS(u'v')$ by all schemes apart from W9. Additionally, the W9 was the only scheme capable of accurately resolving $RS(w'w')$ in the vicinity of y = 0.1. Decreasing the

order of accuracy leads to a gradual shift of the peak location towards the midstream. The wall-normal velocity Reynolds stress $\mathrm{RS}(\mathrm{w'w'})$ is the least accurately captured due to the unresolved turbulent scales associated with the small near-wall fluctuations. Note that the local Mach number of the flow reaches the zero limit as the no-slip wall is approached.

Regarding $\mathrm{RS}(\mathrm{u'v'})$, all schemes overall give a good agreement to the incompressible DNS. All Reynolds stress terms gradually converge to the DNS peak values in the proximity of y = 0.1 ($y^+ \approx 40$), an indication of the prevalence of turbulent production located near the end of the buffer layer.

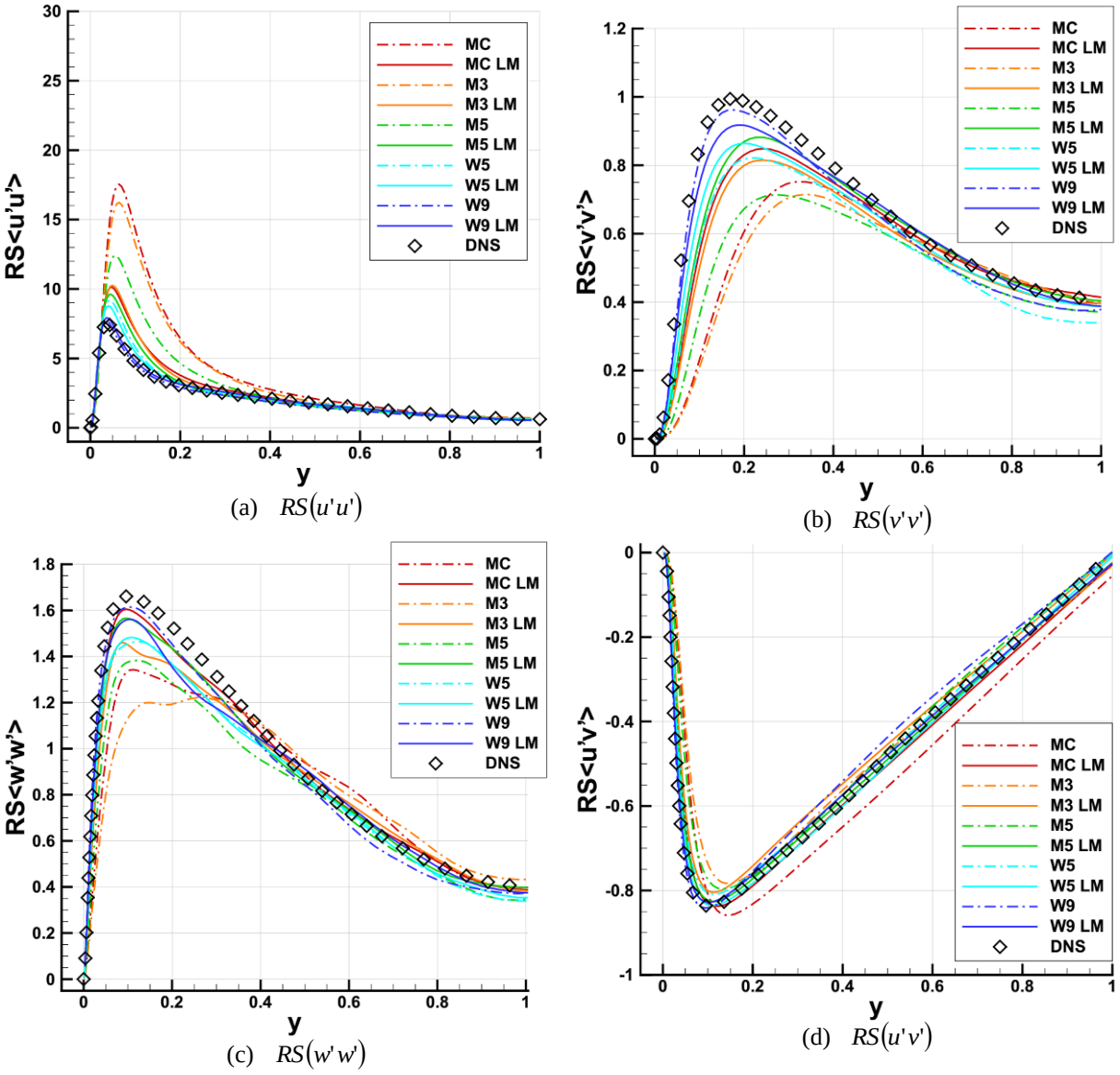

Figure 4: The streamwise velocity Reynolds stresses (RS) calculated by different ILES scheme.

4 COMPRESSION RAMP

4.1 Case parameters

Shock/Turbulent boundary layer interaction (STBLI) over a compression ramp inclined at 24° angle was investigated by Wu and Martin [16] using DNS with free-stream conditions of Mach 2.9 and Re_δ of 38,700. The presence of the inclined surface gives rise to a shock wave, which interacts with the incoming turbulent boundary layer leading to the formation of a separation bubble and a λ-shockwave. The size of the separation region is dictated by the intensity of the incoming turbulent flow and the strength of the formed shock wave. A sketch illustrating the most important physical processes that take place is given in Figure 5.

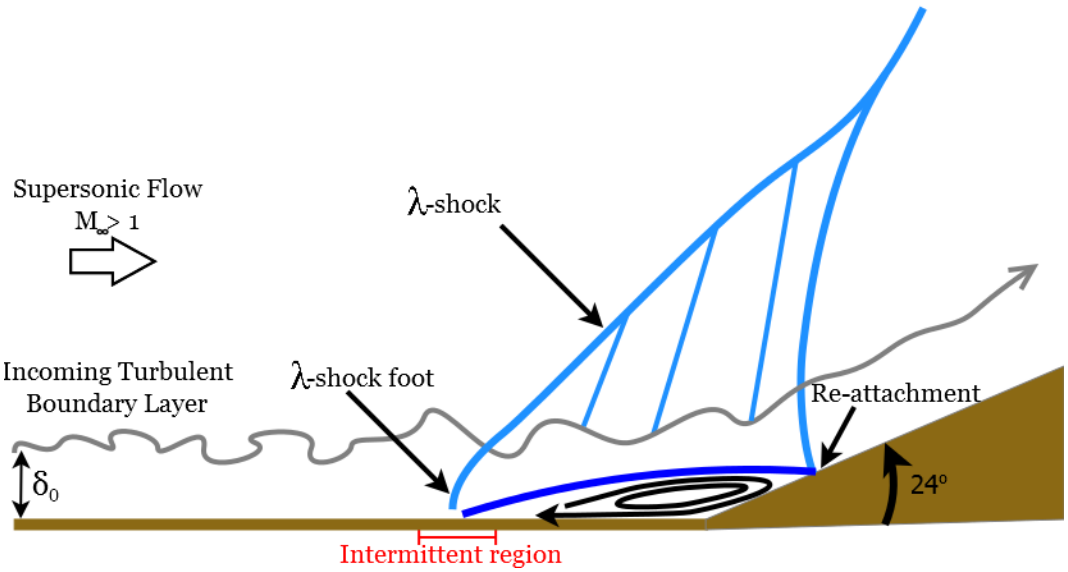

Figure 5: Schematic illustrating the flow over a compression ramp.

The physical properties and computational domain are similar to previous DNS studies and are provided in Table 1 and Table 2, respectively. Since the numerical scheme still needs to capture and resolve the synthetic inflow perturbations that lead to a turbulent flow, the length of the upstream domain is increased relatively to the DNS by approximately five incoming boundary layer heights (δ_0). The spanwise length is also increased in order to investigate possible large-scale structures that may develop in the post-shock region after re-attachment has occurred. Note that henceforth, $x/\delta_0 = 0$ will refer to where the compression corner begins.

δ_0	U_∞	T_∞	Mach	Re_{δ_0}	ρ_∞	T_w
6.4 mm	609.1 m/s	107.1 K	2.9	38,737	0.077 kg/m^3	307 K

Table 1: Flow properties.

Periodic boundary conditions are used in the spanwise (y) direction while in the wall-normal (z) direction a no-slip isothermal wall (T_W=309K) is used. A supersonic outflow condition is imposed at the outlet and upper boundary opposite to the wall. The boundary condition at the inlet requires accurately assigning a turbulent boundary layer. A synthetic turbulent digital filter approach [15], further developed in conjunction with the present numerical study, is employed to generate the incoming turbulent boundary layer data. Apart from the mean turbulent profile data which can be obtained from either previous studies or flat plate simulations,

the digital filter technique requires also knowledge of the integral length scales. Here, an integral length scale of $0.22\delta_0$ is used for the streamwise direction, whereas for the spanwise and wall-normal directions, the integral length scales chosen were $0.2\delta_0$ and $0.5\delta_0$, respectively.

	x_{max}	y_{max}	z_{max}	n_x	n_y	n_z	Δx^+	Δy^+	Δz^+
ILES	21.4	3	5	1128	120	168	41.51	51.92	3.5
DNS[16]	15.4	2.2	5	1024	128	160	31.23	28.56	0.2

Table 2: Mesh parameters for the supersonic ramp flow

4.2 Results

The LM correction is implemented only in conjunction with the 5th-order MUSCL scheme (M5LM). From the WENO schemes examined earlier only the 9th-order WENO variant (W9) will be considered here.

The streamwise distribution of the time and spatially averaged mean wall pressure (Figure 6) shows that the W9 scheme provides more accurate results than the M5LM scheme and is in excellent agreement with both the DNS [16] and experiment [17]. The M5LM scheme (green line) is characterized by a delay in the location of the separation bubble. This is associated with reduced resolution of finer scales compared to W9.

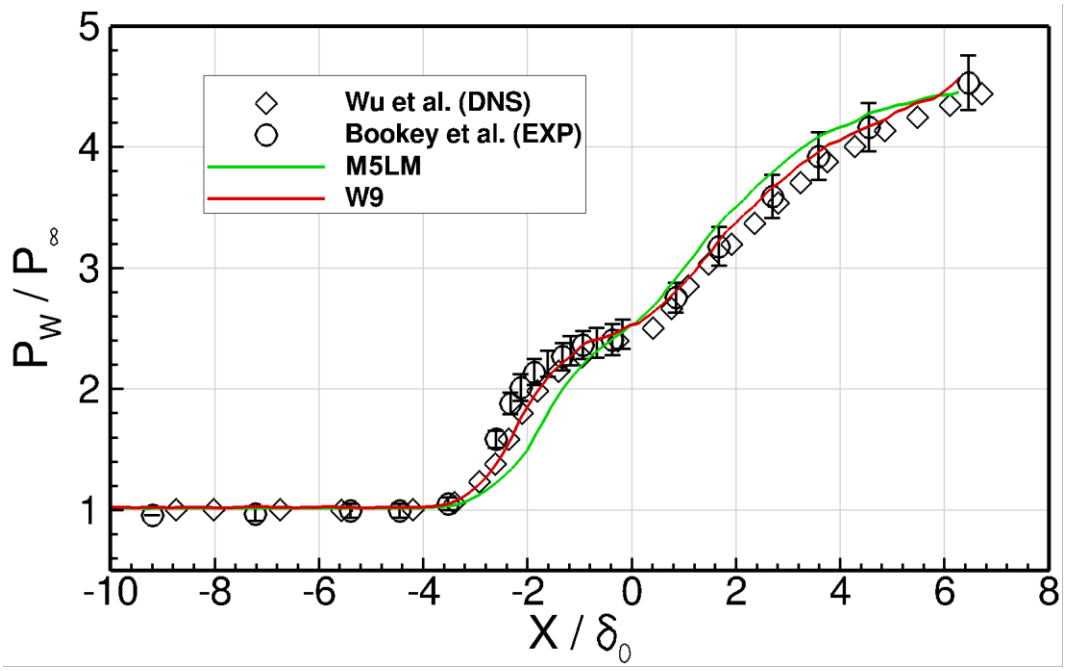

Figure 6: Mean wall pressure distribution in the streamwise direction.

The incoming mean streamwise velocity profile obtained by the digital filter technique at the inflow ($x/\delta_0 = -15$) is compared to a further two downstream locations, positioned at -11 and -8. This allows the observation of the streamwise evolution of the turbulent boundary layer created by the digital filter technique. The position at $x/\delta_0 = -8$ is a common location for both DNS and ILES upstream of the compression ramp corner and STBLI, thus the velocity profiles should closely match. Both M5LM and W9 schemes show very good agreement to the DNS and experiment (Figure 7), however the W9 results are marginally more accurate near the wall ($z/\delta_0 \approx 0.1$) as well as around $z/\delta_0 = 0.5$. Thus, the synthetic turbulent field created by the digital filter technique requires approximately $6\delta_0$ in the streamwise direction to

adjust. The DNS study [16] used the rescaling method developed by Xu and Martin [18] in order to generate the turbulent inflow condition, with the recycling station located at $4.5\delta_0$ downstream of the inlet.

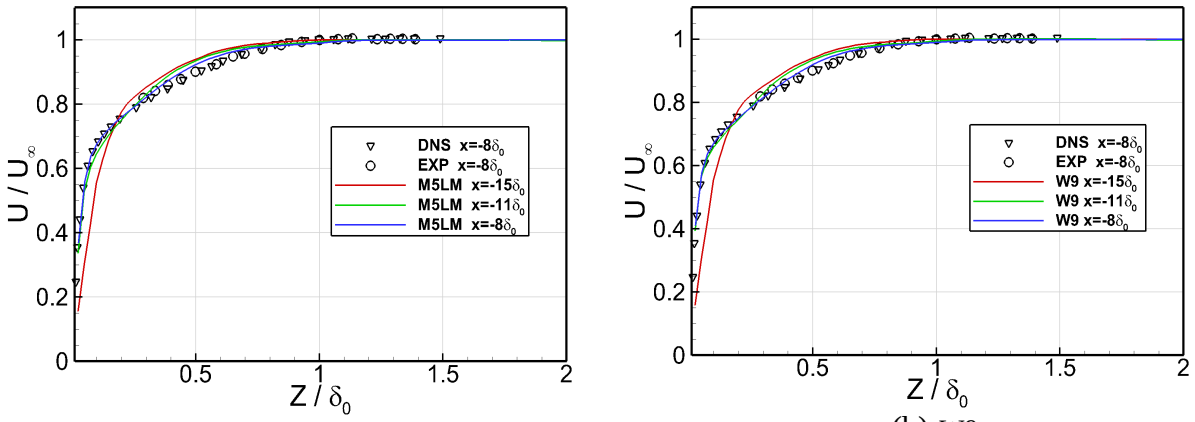

(a) M5LM (b) W9

Figure 7: Comparison of inflow streamwise velocity to the DNS and Experiment using the W9 and M5LM schemes on the fine grid.

By the time the flow reaches the intermittent region where the foot of the λ-shock interacts with the separation bubble formed (Figure 5), there is a considerable difference in the mean streamwise boundary layer profile between the two schemes examined (Figure 8a). The W9 scheme shows the best agreement with the DNS.

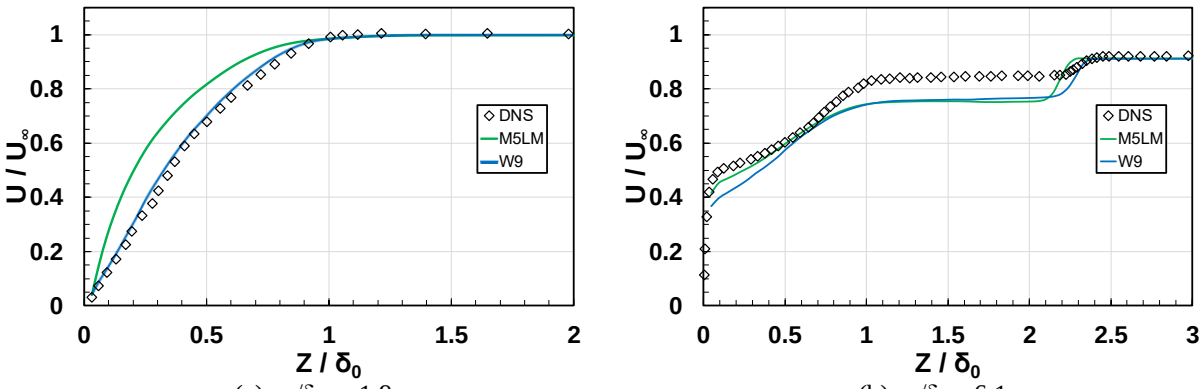

(a) $x/\delta_0 = -1.9$ (b) $x/\delta_0 = 6.1$

Figure 8: Streamwise velocity profiles.

Near the outlet at $x/\delta_0 = 6.1$ (Figure 8b), the velocity profiles of both M5LM and W9 show a noticeable deviation from the DNS. The freestream velocity tangential to the wall ($z/\delta_0 \geq 2.5$) reaches a value similar to DNS both for M5LM and W9 schemes. However, W9 resolves the separation bubble more accurately and consequently the SWBLI region. This is also reflected in the location where the velocity begins to reach the freestream value ($z/\delta_0 \approx 2.3$). Nonetheless, both schemes fail to accurately capture the DNS profile below this point, possibly due to the rapid coarsening of the streamwise grid resolution closer to the outlet.

Figure 9 shows a qualitative comparison between the two numerical schemes with respect to the resolved turbulent flow by plotting the iso-surfaces of the vortex cores. W9 resolves a greater number of vortices than M5LM upstream of the separation region. The differences between the two schemes becomes less apparent downstream of the STBLI.

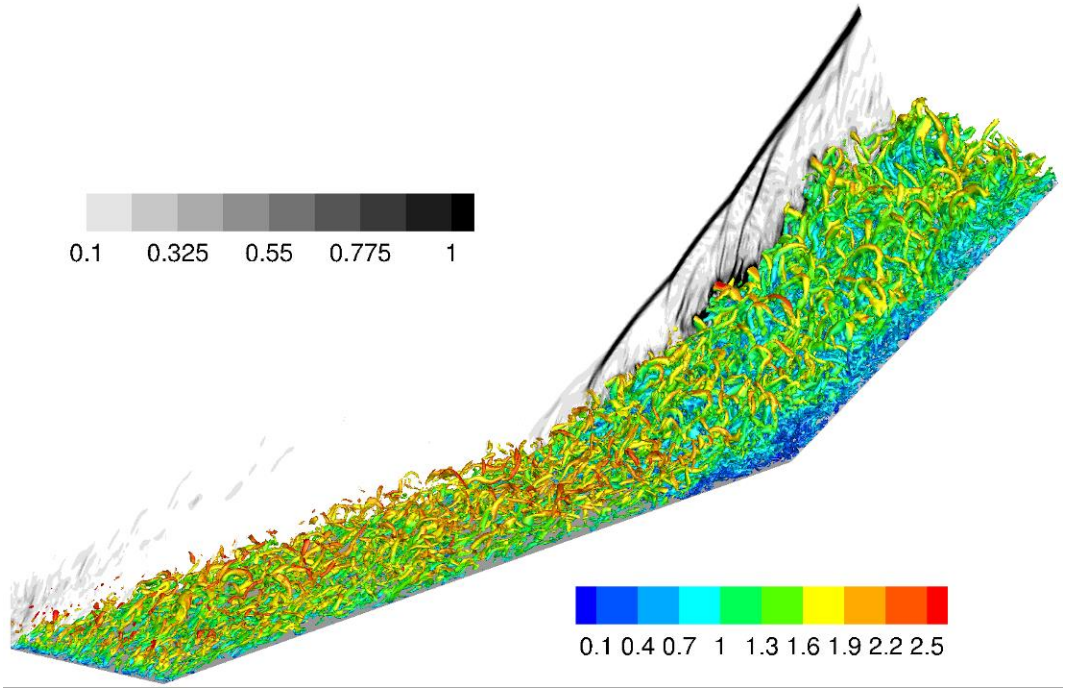

(a) M5LM

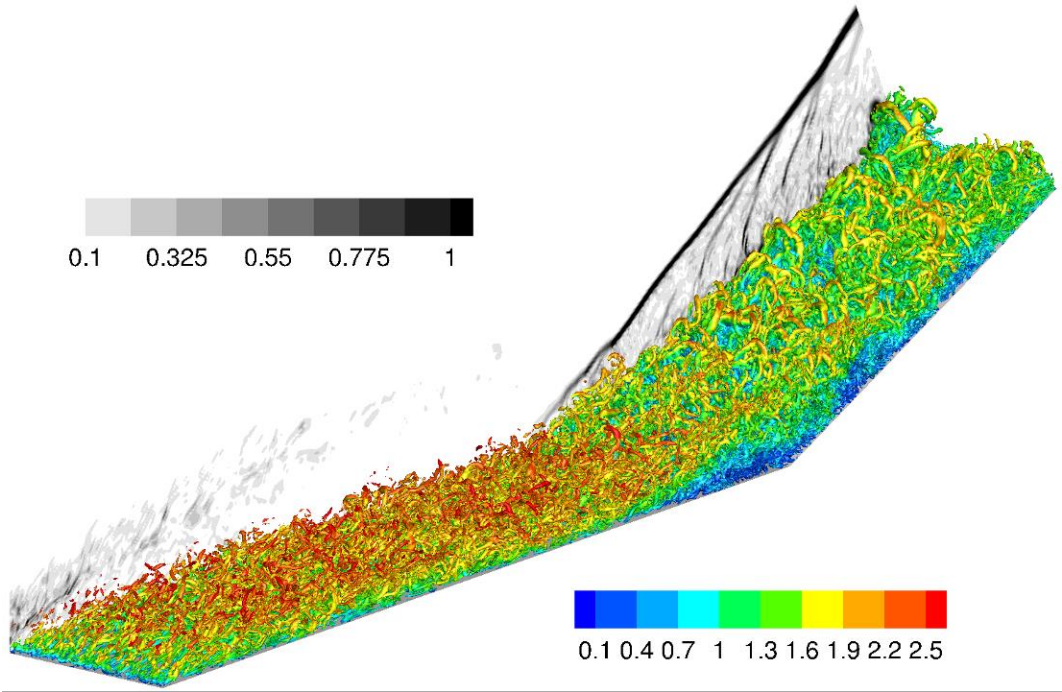

(b) W9

Figure 9: Iso-surfaces of *Q*-criterion $Q = 2\left(\mathrm{U}_{\infty}/\delta_0\right)^2$ coloured by Mach number; grayscale contours plane of density gradient magnitude $\left|\nabla\rho\right|\left(\delta_0/\rho_{\infty}\right)$.

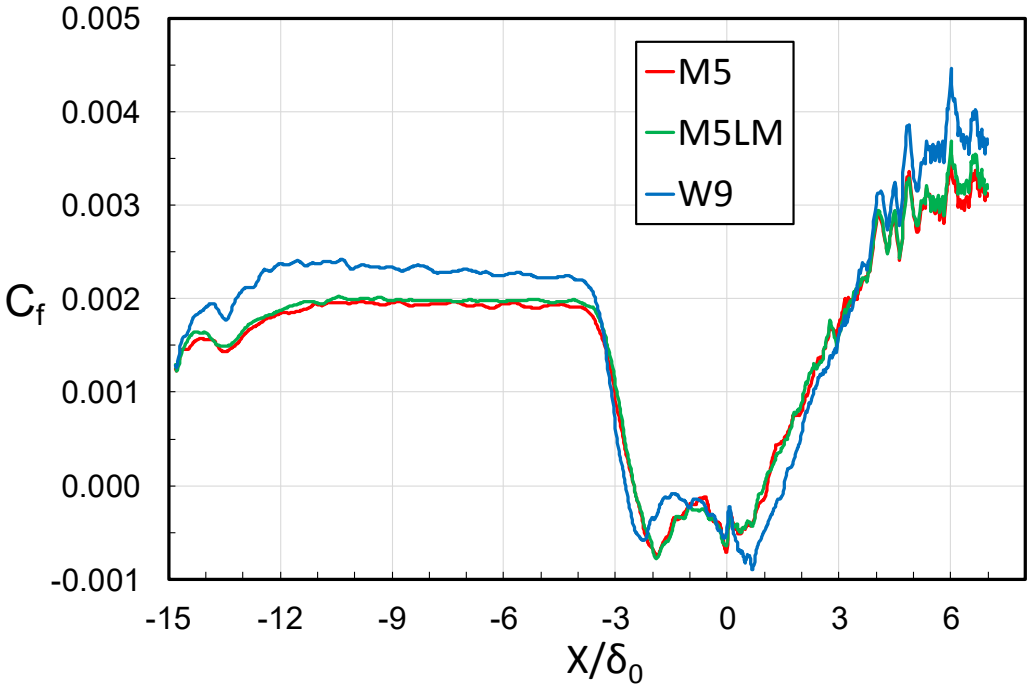

Figure 10: Skin friction coefficient distribution.

Although the flow is supersonic in the freestream, the boundary layer remains subsonic in the first 5 to 10% of the incoming boundary layer height, i.e. approximately 20 computational cells for a relatively fine (LES) grid. The subsonic region of the separation bubble can reach a size of $0.6\delta_0$ and any loss of accuracy here could potentially lead to significant errors. However, the streamwise distribution of the coefficient of friction (C_f) given in Figure 10 suggests that the prediction of separation bubble is primarily influenced by the resolved upstream turbulent boundary layer.

5 CONCLUSIONS

- Low-Mach corrections [5] significantly improve the accuracy of lower order schemes in ILES of subsonic TBL but have little effect on STBLI predictions.
- Low-Mach corrections have a greater effect when they are used in conjunction with lower-order schemes (less or equal to 5th-order).
- Overall, ILES using W9 give very promising results both for subsonic and supersonic turbulent boundary layers.

ACKNOWLEDGEMENTS

Part of this work was sponsored by the Air Force Office of Scientific Research, Air Force Material Command, USAF, under grant number FA9550-14-1-0224. The U.S. Government is authorized to reproduce and distribute reprints for Governmental purpose notwithstanding any copyright notation thereon.

REFERENCES

[1] Toro, E. F. *Riemann solvers and numerical methods for fluid dynamics: a practical introduction, 3rd Edition*. Springer, 2009.

[2] Van Leer, B., Towards the ultimate conservative difference scheme III. Upstream-centered finite-difference schemes for ideal compressible flow. *Journal of Computational Physics*, **23** (3), 263-275, 1977.

[3] Kim, K.H., Kim, C., Accurate, efficient and monotonic numerical methods for multi-dimensional compressible flows: Part II: Multidimensional limiting process. *Journal of Computational Physics*, **208** (2), 570-615, 2005.

[4] Balsara, D.S., Shu, C.-W., Monotonicity preserving weighted essentially non-oscillatory schemes with increasingly high order of accuracy. *Journal of Computational Physics*, **160** (2), 405-452, 2000.

[5] Thornber, B., Mosedale, A., Drikakis, D., Youngs, D., Williams, R.J.R, An Improved Reconstruction Method for Compressible Flows with Low Mach Number Features. *Journal of Computational Physics*, **227,** 4873-4894, 2008.

[6] Kokkinakis, I.W., Drikakis, D., Implicit Large Eddy Simulation of weakly-compressible turbulent channel flow. *Computer Methods in Applied Mechanics and Engineerin*g, **287,** 229-261, 2015.

[7] Spiteri, R.J. and Ruuth, S.J., A New Class of Optimal High-Order Strong-Stability-Preserving Time Discretization Methods. *SIAM Journal on Numerical Analysis*, **40** (2), 469-491, 2002.

[8] Moser, R. D., Kim, J., Mansour, N. N., Direct numerical simulation of turbulent channel flow up to Re_τ=590. *Physics of Fluids*, **11** (4), 943-945, 1999.

[9] Duan, L., Beekman, I., Martin, M.P., Direct numerical simulation of hypersonic turbulent boundary layers. Part 2. Effect of wall temperature. *Journal of Fluid Mechanics*, **655**, 419-445, 2010.

[10] Coleman, G.N., Kim, J., Moser, R.D., A numerical study of turbulent supersonic isothermal-wall channel flow. *Journal of Fluid Mechanics*, **305**, 159-183, 1995.

[11] Morinishi, Y., Tamano, S., Nakabayashi, K., Direct numerical simulation of compressible turbulent channel flow between adiabatic and isothermal walls. *Journal of Fluid Mechanics*, **502**, 273-308, 2004.

[12] Hunt, J.C.R., Wray, A., Moin, P., Eddies, stream, and convergence zones in turbulent flows. *Center for Turbulence Research*, Report **CTR-S88**, 1988.

[13] Fureby, C., Grinstein, F.F., Large eddy simulation of High-Reynolds-number free and wall-bounded flows. *Journal of Computational Physics*, **181** (1), 68-97, 2002.

[14] Tsoutsanis, P., Kokkinakis, I.W., Konozsy, L., Drikakis, D., Williams, R.J.R., Youngs, D., Comparison of structured and unstructured-grid, compressible and incompressible methods using the vortex pairing problem. *Computer Methods in Applied Mechanics and Engineering*, **293**, 207-231, 2015.

[15] Rana, Z.A., Thornber, B., Drikakis, D., Transverse jet injection into a supersonic turbulent cross-flow. *Physics of Fluids*, **23** (4), 2011.

[16] Wu, M., Martin, M.P., Direct Numerical Simulation of Supersonic Turbulent Boundary Layer over a Compression Ramp. *AIAA Journal*, **45** (4), 879—889, 2007.

[17] Bookey, P. B., Wyckham, C., Smits, A. J., Martin, M. P., New Experimental Data of STBLI at DNS/LES Accessible Reynolds Numbers. *43rd AIAA Aerospace Sciences Meeting and Exhibit*, Reno, Nevada, January 10-13, 2005.

[18] Xu, S., Martin, M. P., Assessment of Inflow Boundary Conditions for Compressible Turbulent Boundary Layers. *Physics of Fluids*, **16 (**7), 2623—2639, 2004.